PCCP

ROYAL SOCIETY OF CHEMISTRY

PAPER

View Article Online
View Journal | View Issue

Cite this: *Phys. Chem. Chem. Phys.*, 2024, **26**, 5333

Electrostatically tunable interaction of CO_2 with MgO surfaces and chemical switching: first-principles theory†

Arpita Sen,[a] Ayush K. Narsaria,*[b] Meghna A. Manae,[a] Sharan Shetty[b] and Umesh V. Waghmare*[a]

Electric field-assisted CO_2 capture using solid adsorbents based on basic oxides can immensely reduce the required energy consumption compared to the conventional processes of temperature or pressure swing adsorption. In this work, we present first-principles density functional theoretical calculations to investigate the effects of an applied external electric field (AEEF) within the range from −1 to 1 V Å^{-1} on the CO_2 adsorption behavior on various high and low-index facets of MgO. When CO_2 is strongly adsorbed on MgO surfaces to form carbonate species, the coupling of electric fields with the resulting intrinsic dipole moment induces a 'switch' from a strongly chemisorbed state to a weakly chemisorbed or physisorbed state at a critical value of AEEF. We demonstrate that such 'switching' enables access to different metastable states with variations in the AEEF. On polar MgO(111) surfaces, we find a distinct feature of the adsorptive dissociation of CO_2 towards the formation of CO in contrast to that on the non-polar MgO(100) and MgO(110) surfaces. In some cases, we observe broken inversion symmetry because of the AEEF that results in induced polarity at the interaction site of CO_2 on MgO surfaces. Our results provide fundamental insights into the possibility of using AEEFs in novel solid adsorbent systems for CO_2 capture and reduction.

Received 21st September 2023,
Accepted 3rd January 2024

DOI: 10.1039/d3cp04588a

rsc.li/pccp

1. Introduction

Carbon capture and storage (CCS) is one of the most important technological steps in reducing the carbon footprint to achieve environmentally benign chemical processes.[1] The major contributions to the CO_2 released into the atmosphere are from power plants and transportation.[2] Carbon capture from pre- and post-combustion processes is commercially practiced using the amine solvent process where CO_2 is selectively absorbed by amines.[3,4] This method is energetically demanding due to regeneration cycles and the degradation of amines leading to environmentally unsafe processes.[5,6] In recent years, materials based on solid adsorbents, such as those based on metal oxides, metal organic framework (MOF), and zeolites, have been proposed that have certain advantages over solvent-based technologies.[7,8] The efficiency of solid adsorbents critically depends on the thermodynamics of the adsorption–desorption process. Pressure swing adsorption (PSA) and temperature swing adsorption (TSA) technologies are typically employed for the CO_2 adsorption process for industrial applications.[9–11] However, these technologies can be energy intensive based on the scale of the process. The availability of 'green' electricity produced from renewable sources, such as solar or wind energy, and electric swing adsorption (ESA) could be an attractive technology for CO_2 separation and capture.[12,13] The main advantage of this process is the ambient operation conditions that can avoid large pressure and temperature variations experienced by the solid adsorbents. Another CCS technology that has been gaining traction is external electric field (EEF) swing adsorption.[14–19] EEF can have a significant effect on the adsorption behavior of the molecules on the metal surface due to the dipole change at the interface of the surface+molecule system.[20–24] McEwen and co-workers combined experimental and DFT calculations to demonstrate the applicability of EEFs for steam methane reforming on Ni catalysts.[25,26] They were able to show that in the presence of EEF, coke formation is reduced and the process can operate at lower temperatures. In another study, they discussed the effect of negative and positive EEFs on the reaction towards water dehydrogenation on a Ni surface.[27]

[a] *Theoretical Sciences Unit, Jawaharlal Nehru Centre for Advanced Scientific Research, Jakkur, Bangalore 560064, India. E-mail: waghmare@jncasr.ac.in*
[b] *Shell India Markets Pvt. Ltd, Mahadeva Kodigehalli, Bengaluru, Karnataka 562149, India. E-mail: ayush-kumar.narsaria@shell.com*

† Electronic supplementary information (ESI) available. See DOI: https://doi.org/10.1039/d3cp04588a

Shaik *et al.* discussed their views on the application of oriented EEFs on the reaction kinetics.[28,29] They proposed that the orientation of the EEF was very critical in changing the reaction pathways. Chuah *et al.* showed that CO and H_2 could be desorbed by high electric field pulses to achieve steady-state conditions in the methanol decomposition reaction on rhodium.[30] Keller *et al.*, in a recent study, demonstrated the use of ESA in capturing CO_2 in hollow fibers that have Joule heating properties.[31] In an interesting study on the oxidative coupling of methane reaction, Sugiura *et al.* proved that $Ce_2(WO_4)_3$ supported on CeO_2 exhibited higher selectivity toward C_2 in the presence of an electric field as compared to the conventional process.[32] Shetty *et al.*, in a recent work, combined electric field-based DFT calculations with machine learning algorithms to predict the field-dependent adsorption energies on the Pt(111) surface.[33] These studies provide evidence of the importance of studying electric field-assisted chemical reactions, specifically in the ESA-driven adsorption–desorption processes.

MgO has been recognized as a prototypical basic oxide material for CO_2 capture and storage, mostly due to the abundance of MgO in nature.[34,35] Moreover, due to the presence of the various crystallographic orientations that can be differentiated based on the polarity of the surfaces, MgO can play an important role in its reactivity towards CO_2.[36–43] In a recent computational study, Manae *et al.* showed that CO_2 interactions with various MgO surfaces depend on the local electronic and structural properties of the active site.[35] They proposed that CO_2 interacts weakly with the (100) and oxygen-terminated (111) surface due to the distinct properties of the active sites. It has been proposed in other studies that the reactivity of surface sites towards CO_2 adsorption can be altered by promoters.[44–46] Motivated by this and earlier work on the effects of an applied external electric field (AEEF) on the catalytic properties of molecular adsorption, herein, we investigate the effects of AEEFs on the adsorption behavior of CO_2 on different MgO surfaces.

2. Computational details

We performed first-principles calculations within the framework of plane wave density functional theory (DFT) as implemented in the Quantum ESPRESSO package.[47] A kinetic energy cutoff of 60 Ry was used for the plane wave basis set in the representation of wave functions and a cutoff of 400 Ry was taken to represent the charge density. Interactions between the valence electrons and the core electrons were modelled with the projector augmented wave (PAW) potentials.[48] We have used the revised exchange–correlation energy of the Perdew–Burke–Ernzerhof (PBEsol) functional within a generalized gradient approximation (GGA).[49] The occupation numbers of electronic states were smeared with the Fermi–Dirac distribution with a smearing width (k_BT) of 0.04 eV. We have included van der Waals (vdW) interactions using the Grimme scheme.[50] Equilibrium structures were obtained through the minimization of energy until the Hellmann–Feynman forces on each atom were smaller than 7×10^{-6} eV Å^{-1} in magnitude. The various surfaces of MgO were modelled by periodic supercells, including a vacuum layer of 15 Å thickness parallel to the slab separating its adjacent periodic images. Each supercell contains a slab of 5 atomic planes, with each plane of the surface containing 3×3 in-plane units. In bare surface calculations, all 5 atomic planes were optimized. Adsorption calculations were performed by freezing the bottom 2 atomic planes while relaxing only the top 3 planes with the CO_2 adsorbate (please check the Computational details section in the ESI,† for further details). Brillouin zone integrations were performed with a uniform grid of $4 \times 4 \times 1$ k-points for all surfaces. We optimized the structures of bare MgO surfaces, the surfaces with CO_2 molecules, and the isolated CO_2 molecule, including an external electric field ranging from -1.0 to 1.0 V Å^{-1}. Although such high electric fields could be difficult to realize in controlled experiments, there are a few good reasons for us to choose such a magnitude of electric fields. Che *et al.* showed in a combined computational and experimental study that large electric fields are necessary for altering the adsorption energy of molecular species such as H_2O and OH. A high electric field is needed to change the electronic states of the adsorbates and the surface for field-induced chemisorption.[51,52] Large electric fields can also be observed in the electrochemical cells at the electrode and the electrolyte interface.[51,53] Moreover, AEEFs used in DFT simulations are typically large because they correspond to low temperatures ($\sim$0 K) and in the absence of any pressure. A high AEEF is needed to cross the barrier separating one metastable state from another. Under experimental conditions, thermal fluctuations facilitate such a crossover at a lower electric field. To simulate the response of MgO to an electric field, we added a saw-tooth potential as a function of z (perpendicular to the surface). The electric field was applied using a saw-tooth potential with a sharp, short step in the middle of the vacuum. The slope of the saw-tooth potential is the electric field. Dipole corrections were included to eliminate the effects of a polar field arising from the continuity and periodicity of the electrostatic potential.[54]

We have calculated the adsorption energy (E_{ad}) of CO_2-adsorbed MgO surfaces with varying electric fields, *i.e.*, ranging from -1 to 1 V Å^{-1} and an interval of 0.1 V Å^{-1}, unless otherwise mentioned. The E_{ad} is defined as follows:

$$E_{ad} = E_{surface+molecule} - E_{surface} - E_{molecule} \quad (1)$$

The E_{ad} values at a given electric field were evaluated by separately calculating the three terms (see eqn (1)) at a given electric field E_z. Structures corresponding to higher negative E_{ad} values possess greater stability. E_{ad} was calculated for MgO(100), (110), and Mg and O-terminated (111) surfaces, referred to as 111-Mg and 111-O surfaces, respectively, with the CO_2 molecule on three sites (Mg-top, O-top and bridge site) on each of the MgO surfaces as shown in Scheme 1. We determined the E_{ad} of these twelve configurations with varying electric fields.

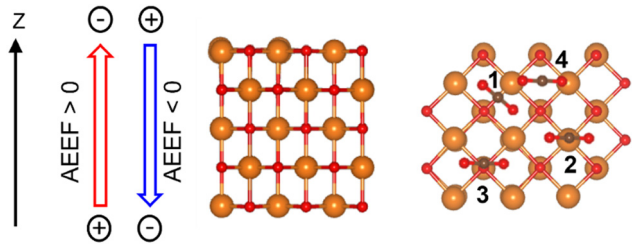

Scheme 1 A schematic diagram depicting the electric field AEEF along the z-axis of the MgO slab (side view in left figure) and the different adsorption configurations of CO_2 on MgO surfaces (right figure) at the bridge site (1), Mg-top site (2), O-top site (3), and hollow site (4).

3. Results and discussion

3.1 MgO(100) surface

The MgO(100) surface has the lowest surface energy among the four MgO surfaces considered here and hence is the most stable and dominant surface of the rocksalt crystals of MgO.[35] Fig. 1 describes the change in the adsorption energy of CO_2 on the (001) surface with respect to the AEEF. In the absence of the AEEF, CO_2 is adsorbed on the bridge site (Fig. 1(b)) with an E_{ad} of −1.0 eV, where the CO_2 is bent with an O–C–O angle of 133°. The C atom of CO_2 interacts strongly with the surface O atom, indicating the formation of carbonate species where the more electronegative O atoms of CO_2 interact with Mg atoms on the surface. Starting with strong adsorption at a negative AEEF, the adsorption energy increases linearly and gradually with the AEEF until it reaches 0.202 V Å^{-1}. Such a linear variation of energy with the AEEF confirms that the inversion symmetry of the adsorption site is broken due to the AEEF giving rise to an induced dipole moment. Interestingly, at 0.203 V Å^{-1} there is a sudden step change in the adsorption energy from −0.79 to −0.4 eV. Examination of the structural evolution with the AEEF reveals that the CO_2 molecule remains bent from −1.0 till 0.202 V Å^{-1} and essentially detaches from the bridge site at 0.203 V Å^{-1}, changing to a weakly adsorbed state (Fig. 1(d) and Fig. S2, ESI†). The O–C–O bond angle changes from 134° to 169° and the O of the MgO slab and the C of the CO_2 bond length increase from 1.45 to 2.38 Å (see Fig. S1 and S2, ESI†). The adsorption energy attains a plateau beyond AEEF of 0.203 V Å^{-1}. This shows that the CO_2 molecule is in a weakly bound state on the MgO surface beyond an AEEF of 0.203 V Å^{-1}.

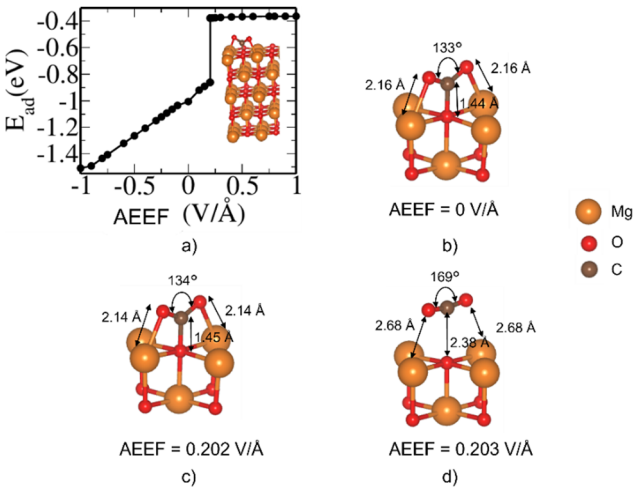

Fig. 1 (a) Variation of adsorption energy (eV) with respect to the AEEF (V Å^{-1}). (b)–(d) The optimized structures of CO_2 adsorbed on the bridge site of Mg(100) at AEEFs of 0, 0.202 and 0.203 V Å^{-1}, respectively.

The $E - E_0$ defined in Fig. 2 is the total energy difference with AEEF (E) and without AEEF (E_0). We can see that the energy of the bare surface (Fig. 2(a)) and of the molecule (Fig. 2(b)) is a quadratic function of AEEF (symmetric parabola), while the CO_2 adsorbed on the surface state has a discontinuity at 0.203 V Å^{-1}. To gain further insight into this discontinuity, we examined the behavior of $E_{surface+molecule}$ with positive and negative electric fields separately, as shown in Fig. 2(d) and (e). The linear term ($b.E$ in eqn (2)) corresponds to the energy of the electric field interacting with the dipole moment (b in $b.E$ or the dipolar energy). The dipolar energy changes significantly in these two regions (see Fig. 2(d) and (e)). The noticeable change in the $E_{surface+molecule}$ value at 0.203 V Å^{-1} therefore originates from the change in dipole moment that arises from the bending of CO_2. It should be noted that the quadratic term ($c.E^2$ in eqn (2)) that accounts for polarizability (c in $c.E^2$) is about the same in these two regions.

$$E_{ad} = a + b.E + c.E^2 \quad (2)$$

Such a jump in electric dipole moment is analogous to polarization switching in ferroelectric materials.[55,56] Here, it is associated with a change in the chemical structure of CO_2. We thus inferred that the CO_2 molecule chemically 'switches' from a strongly to a weakly adsorbed state at AEEF = 0.203 V Å^{-1}. Starting with the relaxed structure obtained at 0 electric field, we thus found two distinct metastable structures upon relaxation at AEEFs of 0.202 V Å^{-1} and 0.203 V Å^{-1}, driven by the interaction of the dipole moment of CO_2 with the AEEF.

The adsorption of CO_2 on the Mg site of the Mg(100) surface shows rather contrasting behavior as evidenced in Fig. 3(a) when compared to the adsorption on the bridge site discussed above. The large fluctuations or the jumps in adsorption energy, as seen in Fig. 3a, is because there are three metastable structures, labeled C, A_h and B_{Mg}, which switch from one to another with the AEEF. For a particular metastable structure (for example C), the adsorption energy varies linearly with the AEEF. This linear component in the variation of adsorption energy with the AEEF is associated with the interaction of the dipole moment with the AEEF. This is true for all three metastable structures (please see the dashed lines in Fig. 3a). With the AEEF, one can transition or switch from one metastable state to another. The first region is designated as A_h, which corresponds to the E_{ad} around −0.4 eV and is an intermediate adsorbed state; the second region (B_{Mg}) is a weakly bound state around $E_{ad} \sim -0.1$ eV, and the third region (C) is a strongly adsorbed state corresponding to $E_{ad} < -0.8$ eV. The most stable state at AEEF = 0.0 V Å^{-1} belongs to the first kind, *i.e.*, A_h, where CO_2 gets adsorbed at the hollow site. As the

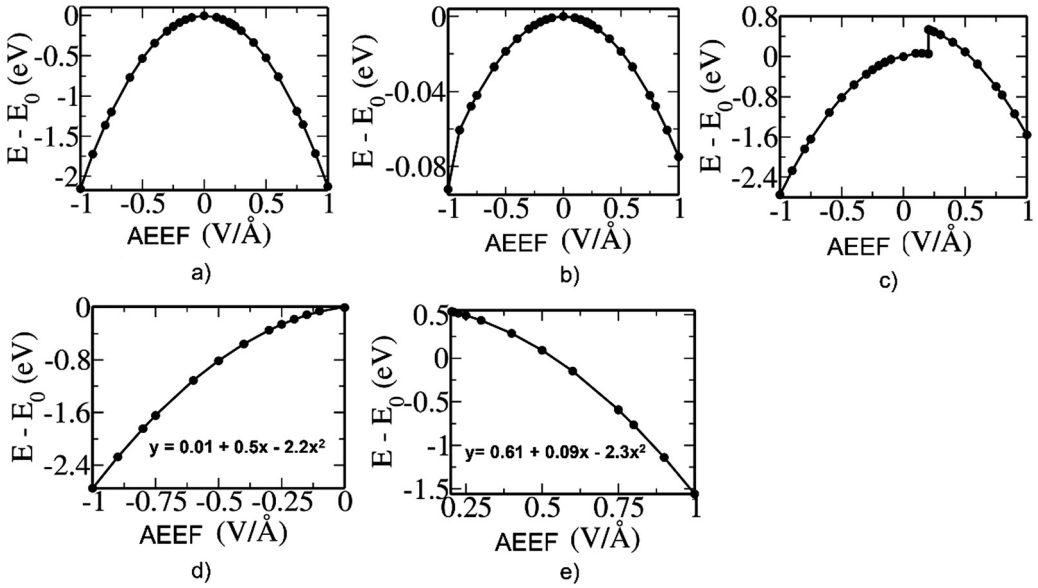

Fig. 2 Contribution of each term (see eqn (1)) to the energy of adsorption at different AEEF: Variation of electronic energy of (a) the bare MgO(100) surface, (b) isolated CO_2 molecule and (c) CO_2 adsorbed on the bridge site of the MgO(100) slab with AEEF relative to the case with zero AEEF. Quadratic fit of energy *vs.* AEEF for the CO_2 adsorbed on the MgO surface with (d) negative and (e) positive AEEF (see eqn (2)).

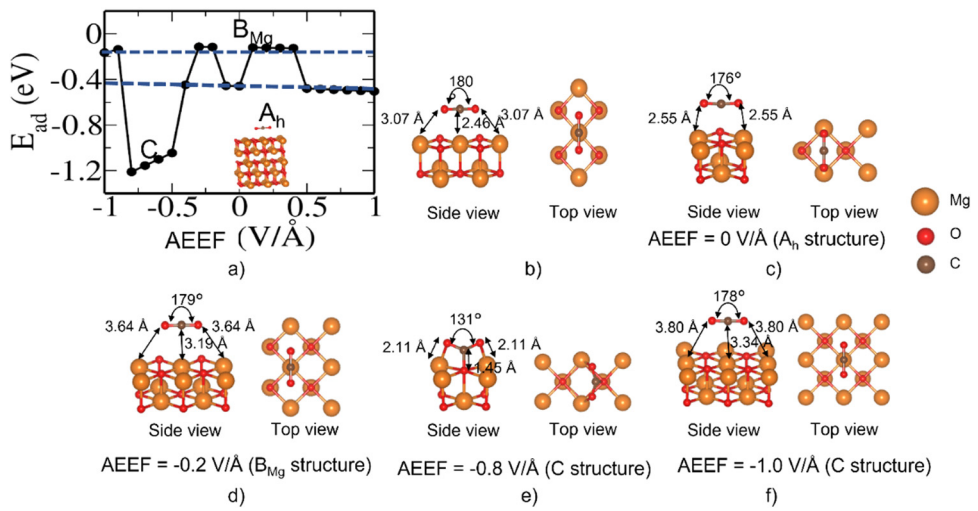

Fig. 3 (a) The dependence of E_{ad} (in eV) on the AEEF of MgO(100)/CO_2 on the Mg top site. (b) The initial structure; the relaxed structures at AEEFs of (c) 0.0 V Å^{-1} (the set of structures marked as A_h), (d) −0.2 V Å^{-1} (set of structures marked as B_{Mg}), (e) −0.8 V Å^{-1} (set of structures marked as C), and (f) at −1.0 V Å^{-1} (set of structures marked as C).

AEEF shifts to the negative field (from ∼−0.1 to −0.5 V Å^{-1}), the E_{ad} proceeds through a transition from the A_h region to B_{Mg} to A_h. We also observed that the CO_2 molecule shifts from a hollow site (Fig. 3(c)) to the Mg top site (Fig. 3(d)) where the CO_2 is displaced vertically upwards minimizing the interaction with the surface. At an AEEF of around −0.5 V Å^{-1} to −0.8 V Å^{-1}, the magnitude of E_{ad} increases (more negative) in the range of −1.0 eV to −1.2 eV (Region C). The CO_2 adsorbed state in Region C indicates carbonate formation, where CO_2 bends and forms a strong bond with the surface O (Fig. 3(e)). Surprisingly, at an AEEF of around −1.0 V Å^{-1}, we noticed that the state of adsorption switched to the B_{Mg} type, *i.e.*, a weakly adsorbed state (Fig. 3(f)). At the positive AEEF field, we observed only B_{Mg} and A_h regions. However, at AEEF > 0.5 V Å^{-1}, CO_2 preferentially remained in the relatively weakly bound A_h state. The structures C and B_{Mg} switched at AEEF = −1.0 V Å^{-1}. Relaxation of the structure type C at AEEF = −1.0 V Å^{-1} leads to no qualitative change in the structure (preserving the C-type structure, see the details given in the ESI†).

The states of CO_2 adsorption at the O site of the Mg(100) surface (Fig. 4) can be classified into two types of states, *viz.*, Region I: E_{ad} < −0.6 eV, and Region II: E_{ad} > −0.6 eV. In the

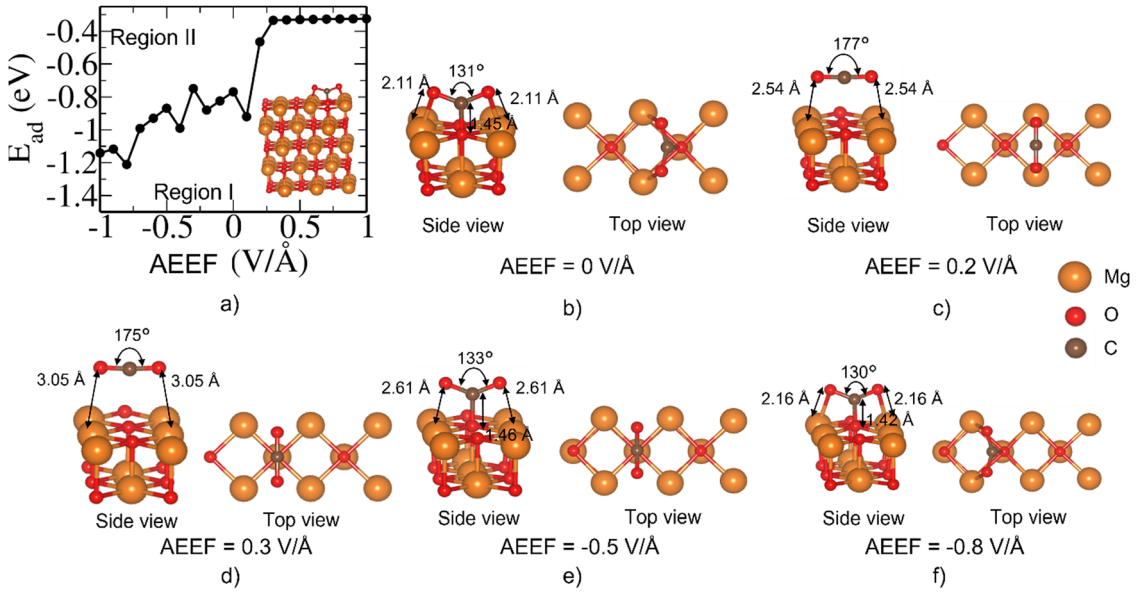

Fig. 4 (a) The variation in E_{ad} (in eV) of MgO(100)/CO_2 on the O top site with AEEF. The relaxed structure at AEEFs of (b) 0.0 V Å^{-1}, (c) 0.2 V Å^{-1}, (d) 0.3 V Å^{-1}, (e) −0.5 V Å^{-1} and (f) −0.8 V Å^{-1}. E_{ad} has been classified into two regions, Region I (E_{ad} < −0.6 eV, more stabilizing) and Region II (E_{ad} > −0.6 eV, less stabilizing), respectively.

former, E_{ad} has a rich behavior where it passes through several energy maxima/minima (Fig. 4(a)), particularly at a negative AEEF, and attains a stable state at around AEEF = −1 V Å^{-1}, corresponding to E_{ad} of ∼−1.2 eV. These several adsorption states are separated by an E_{ad} of ∼0.4 eV (see Fig. 4(a)). From these results, we infer that the CO_2 molecule experiences different low-lying minima at negative AEEFs (accessible with AEEF and small perturbations). The structures (Fig. 4(e) and (f)) correspond to Region I where the C of the CO_2 interacts with the O of the MgO surface, and the CO_2 is bent to enable a favorable interaction with MgO. In Region II, E_{ad} becomes less stabilizing and reaches a constant value of −0.3 eV for AEEF > 0.3 V Å^{-1}. Consequently, the O–C–O bond angle shifts from a bent configuration (130°) at AEEF = 0 V Å^{-1} to linear (175°–177°) as the AEEF becomes positive. Broadly, we find here two types of metastable structures, the MgO slab with linear CO_2 and the MgO slab with bent CO_2. The details are given in the ESI.†

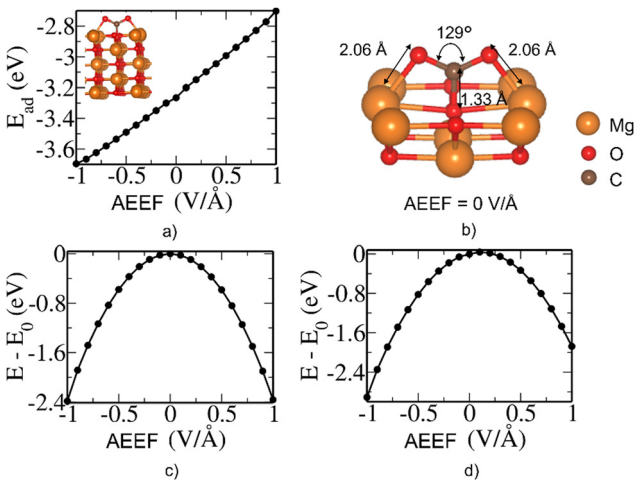

Fig. 5 (a) The variation of E_{ad} (in eV) with the AEEF for MgO(110)/CO_2 on the O top site. (b) The relaxed structure at zero AEEF. The variation of the electronic energy (in eV) of the (c) bare (110) surface and (d) CO_2 adsorbed on the O site of the (110) MgO surface with the AEEF relative to the case with zero AEEF.

3.2 MgO(110) surface

We now consider the MgO(110) surface that is less stable (higher surface energy by 0.4 eV Å^{-2}[12]) than the MgO(100) surface and is highly reactive towards CO_2 adsorption compared to the (100) surface.[42] We obtained optimized structures starting with CO_2 on top of the O site, Mg site, and bridge site. At AEEF = 0 V Å^{-1}, we find that the CO_2 molecule has an adsorption energy of −3.2 eV and forms CO_3^{2-} species (Fig. 5(b)) when relaxed from the O top site. We see a linear relationship between the AEEF and E_{ad} (Fig. 5(a)) in contrast to the switching seen in the case of the MgO(100) surface. As there are no accessible metastable states in our analysis presented in Fig. 5, there are no fluctuations or jumps in E_{ad} with AEEF. The quadratic variation or a slight deviation from the linear variation in the adsorption energy with AEEF is attributed to polarizability (or dielectric constant of MgO), which causes a dipole moment induced by AEEF. The total energy difference with and without AEEF, *i.e.*, $E - E_0$, of the pristine MgO(110) slab (Fig. 5(c)) and CO_2 adsorbed on the slab on the O of MgO (Fig. 5(d)) is a quadratic function for the (110) surface similar to the (100) surface. However, there is no discontinuous change in E_{ad} for CO_2 adsorption on the (110) surface in contrast to that on the (100) surface (Fig. 2(c)). The structure of CO_2 in the adsorbed state at AEEF in the range from −1 to 1 V Å^{-1} does not change and qualitatively remains in the same CO_3^{2-} state, as

described in Fig. 5(b). It is clear that the changes in E_{ad} seen in Fig. 5(a) without many structural changes are due to the difference in the $E - E_0$ of the bare MgO(110) surface (Fig. 5(c)) and the CO_2-adsorbed MgO(110) surface (Fig. 5(d)). One should note that the CO_2 contribution to E_{ad} is relatively weaker, as shown in Fig. 2(b). To understand the orbitals involved in the interaction of the CO_2 molecule with the MgO surface, we considered a configuration of CO_2 interacting with the MgO(110) surface adsorbed on the O site at an AEEF of 0.1 V Å^{-1}. From the partial density of states, the specific occupied state (overlapping with the valence band) that has contributions from orbitals of the CO_2 molecule was identified. Visualization of an isosurface of charge density associated with this state at the *Y*-point shows that the HOMO of CO_2, which is essentially the lone pair p-orbitals of its O atoms, interacts with Mg atoms of the MgO(110) surface, and the p-orbitals of O atoms on the MgO surface interact with the C atom of the adsorbed CO_2 molecule, leading to the formation of the CO_3^{2-} state (see Fig. S5, ESI†).

We also explored the adsorption of CO_2 on the Mg site (Fig. 6(b)) of the MgO(110) surface. The CO_2 molecule shifts to the O site in the relaxed structure at AEEF = 0 V Å^{-1} resulting in the formation of a CO_3^{2-}-like structure (see Fig. 5(b)). At an AEEF of −0.1 V Å^{-1}, CO_2 desorbs (Fig. 6(d)) and remains in that state till −0.4 V Å^{-1}, and the desorbed state switches back to the adsorbed state at AEEF = −0.5 V Å^{-1} with E_{ad} of −3.5 eV. Surprisingly, at AEEF = −0.8 V Å^{-1}, the structures switch back to the desorbed state. While there are oscillations in the adsorption energy behavior at negative AEEF, it exhibits a linear variation at positive AEEF, remaining in the CO_3^{2-} state (Fig. 6(a)). Oscillation in the CO_2 adsorbed state (at the Mg site (Fig. 6)) is intriguing and probably reflects local energy minima, in contrast to adsorption at the O site (Fig. 5), while the two states are structurally similar. Thus, we found three metastable states, and their switching and structural transformations are discussed in detail in ESI.†

Optimization of CO_2 on the bridge site of the MgO(110) results in the formation of the CO_3^{2-} state (AEEF = 0) as shown in Fig. 7(c), which is accompanied by the local reconstruction of the surface near the adsorption site. This state remains unchanged at the AEEF from −1.0 V Å^{-1} to 0.2 V Å^{-1}. Around AEEF = 0.3 V Å^{-1}, the CO_3^{2-} state is further stabilized due to the favorable orientation of the bent CO_2 relative to the surface. Remarkably, at 1.0 V Å^{-1}, CO_2 destabilizes and desorbs from the surface (Fig. 7(f)). We thus find here two metastable states that are accessible with the AEEF ranging from −1.0 to 1.0 V Å^{-1}, upon relaxation starting from the structure stable at 0 V Å^{-1}. The details are given in ESI.†

3.3 MgO(111) surface

The MgO(111) surface is the least stable and the most interesting in the context of the reactivity of CO_2 adsorption due to the polarity of the surface, unlike its (100) and (110) surfaces.[41,42] Considering the polarity of the MgO(111) surface, the reactivity of the surface depends on the surface orientation, *i.e.*, Mg or O termination. We will discuss simulations of CO_2 adsorption on these surface orientations in the presence of AEEF. Fig. 8 describes the adsorption behavior of CO_2 on the Mg top site of the Mg-terminated MgO(111) surface with varying AEEF. CO_2 adsorbed very weakly at AEEF from 1 V Å^{-1} till −0.6 V Å^{-1} (Fig. 8(a)). The structures of CO_2 on the Mg-terminated MgO(111) surface (Fig. 8(b) and (c)) corresponding to AEEFs ranging from 1.0 to −0.6 V Å^{-1} confirmed its weak adsorption on the surface. At an AEEF of −0.7 V Å^{-1}, drastic stabilization of

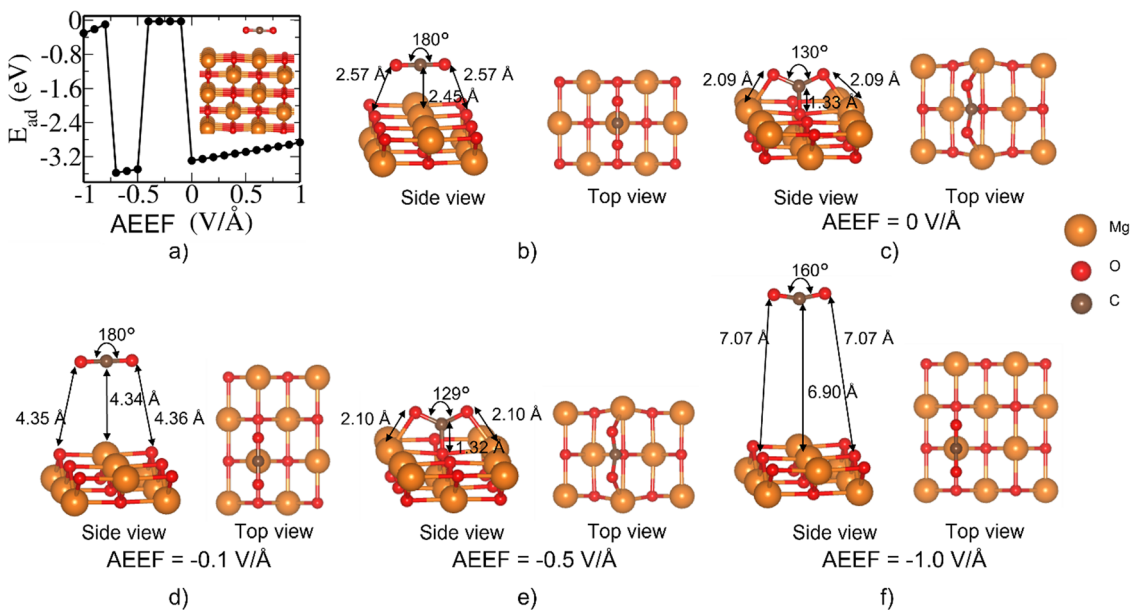

Fig. 6 (a) The variation of E_{ad} (in eV) with the AEEF for MgO(110)/CO_2 on the Mg top site. (b) The initial structure with CO_2 on the Mg site. The relaxed structures of the configurations at AEEFs of (c) 0.0 V Å^{-1}, (d) −0.1 V Å^{-1}, (e) −0.5 V Å^{-1}, and (f) −1.0 V Å^{-1}. Small adsorption energies in (a) represent weakly adsorbed states with long distances between CO_2 and the surface (*e.g.* (d) and (f)).

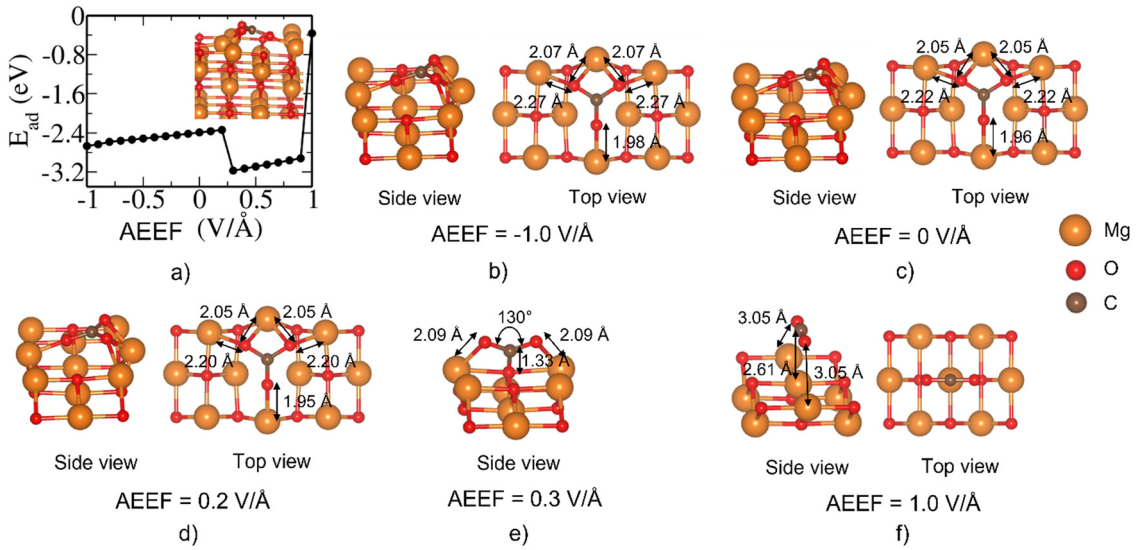

Fig. 7 (a) The variation of E_{ad} (in eV) with the AEEF for MgO(110)/CO_2 on the bridge site. Relaxed structures of the configurations at AEEFs of (b) 0.0 V Å^{-1}, (c) 0.2 V Å^{-1}, (d) 0.3 V Å^{-1}, (e) 1.0 V Å^{-1}, and (f) -1.0 V Å^{-1}.

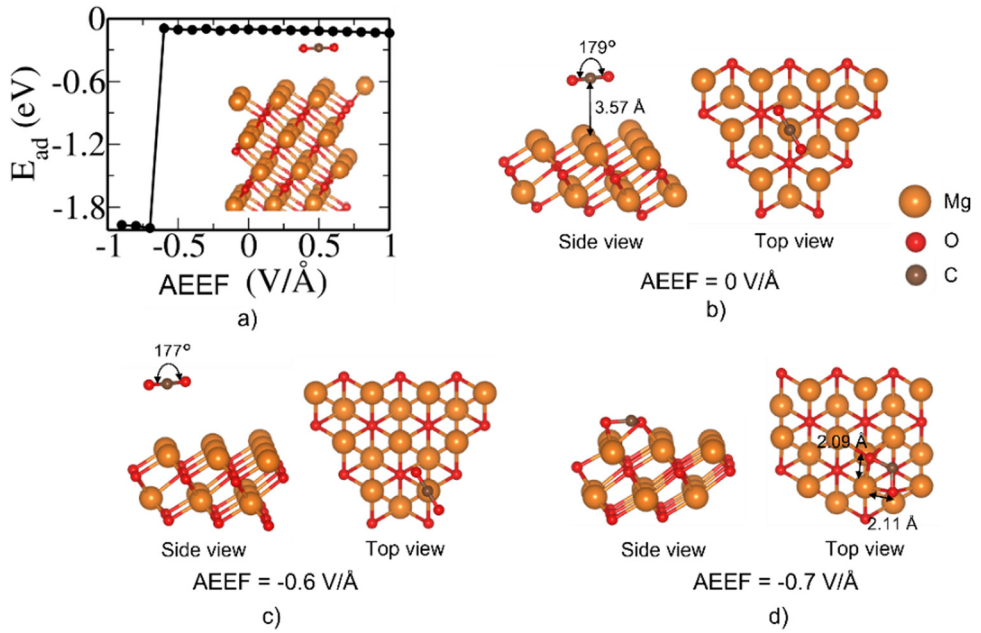

Fig. 8 (a) The variation of E_{ad} (in eV) with AEEF on MgO(111)-Mg-terminated/CO_2 on the Mg top site. Relaxed structures of configurations at AEEFs of (b) 0.0 V Å^{-1}, (c) −0.6 V Å^{-1}, and (d) −0.7 V Å^{-1}.

CO_2 on the surface was observed. Fig. 8(d) indicates that the CO_2 forms a carbonate compound and is adsorbed on the MgO slab with the O atoms of CO_2 interacting strongly with the surface Mg atoms. This state remains unchanged until an AEEF of −1 V Å^{-1}. We found here two metastable states of CO_2 adsorbed on the Mg-terminated (111) surface and a structural transformation at AEEF −0.7 V Å^{-1}. The details are given in the ESI.†

CO_2 adsorption at a bridge site of the Mg-terminated (111) surface is weak at AEEF = 0 V Å^{-1}, similar to the adsorption over the Mg top site, as discussed above. At 0 V Å^{-1}, CO_2 is aligned horizontally (parallel to the surface) over the bridge site with its O atoms facing the Mg atoms (Fig. 9(b)), in contrast to the case where the C of the CO_2 is on top of the Mg atom (Fig. 8(b)). Surprisingly, CO_2 can further undergo an irreversible dissociative adsorption into CO + O (Fig. 9(c)) at AEEF = 0.5 V Å^{-1}. The CO fragment in the dissociated state is aligned perpendicular to the surface and its O atom is bonded to the Mg atom (see Fig. 9(c)). It is interesting to note that the CO species from the dissociated state is weakly adsorbed on the surface with C–Mg bond lengths of ∼2.3 A, or, in other words, the CO formed could be easily desorbed. More details on the structural transformation can be found in the ESI.†

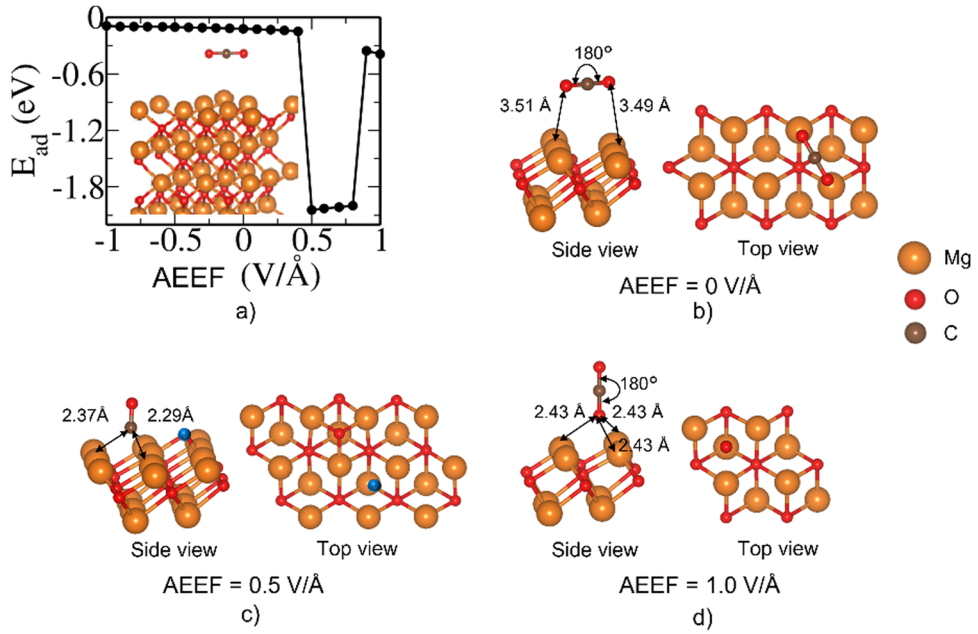

Fig. 9 (a) The variation of E_{ad} (in eV) with the AEEF for MgO(111)-Mg-terminated/CO_2 on the bridge site. Relaxed structures of configurations at AEEFs of (b) 0.0 V Å^{-1}, (c) 0.5 V Å^{-1}, and (d) 1.0 V Å^{-1}. The dissociated O from CO_2 in (c) is colored blue.

We believe that the contribution to the higher adsorption energy is from the O adsorption on the Mg atoms rather than the interaction of the CO with the surface. With AEEF = 0.9 V Å^{-1}, the CO_2 molecule goes back to a weaker adsorption state (Fig. 9(a)), where the CO_2 is linearly oriented over the MgO surface (Fig. 9(d)). We find here 3 types of structures with significant structural transformation at the AEEFs of 0.5 V Å^{-1} and 0.9 V Å^{-1}. The details are given in the ESI.†

We also evaluated the adsorption of CO_2 on two sites, *viz.*, the bridge and top (Fig. 10 and 11) of the O-terminated MgO(111), *i.e.*, the MgO(111)-O surface. It is clear that CO_2 adsorption on the MgO(111)-O surface shows distinct behavior as compared to the Mg-terminated MgO(111) surface.

At AEEF from −1 to 0.3 V Å^{-1}, there is a very weak adsorption of CO_2 on the bridge site of the MgO(111)–O surface; the CO_2 remains relatively flat (O–C–O bond angle of 178°, see Fig. 10(b)). However, at AEEF = 0.4 V Å^{-1}, the CO_2 molecule undergoes dissociation into CO + O and the adsorption energy stabilizes below −6 eV as seen in (Fig. 10(a)). CO_2 remains dissociated for AEEF > 0.4 V Å^{-1}. This drastic change in the

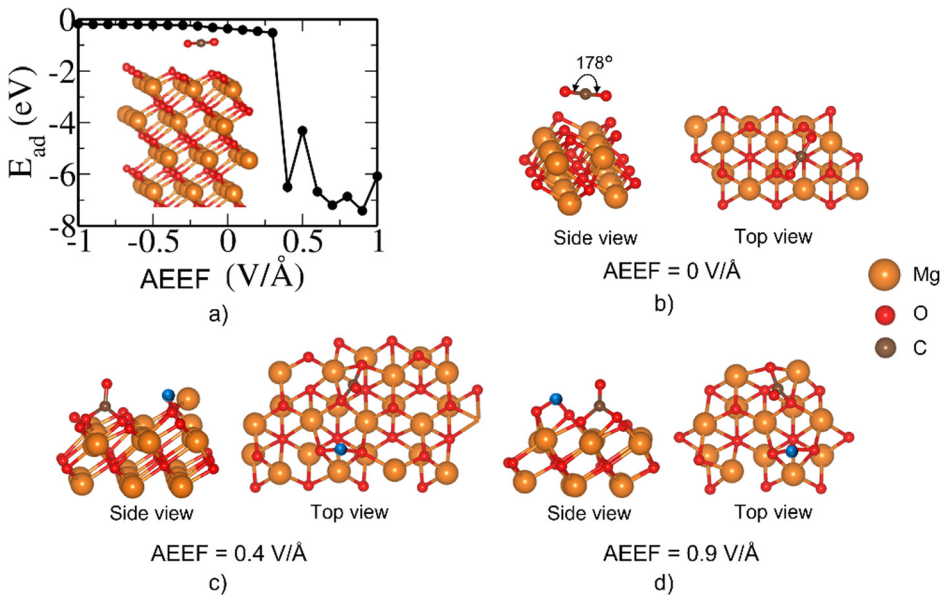

Fig. 10 (a) The variation of E_{ad} (in eV) with AEEF for MgO(111)–O-terminated/CO_2 on the bridge site. Relaxed structures of configurations at (b) 0.0 V Å^{-1}, (c) 0.4 V Å^{-1}, and (d) at 0.9 V Å^{-1}. The dissociated O from CO_2 in (c) is colored blue.

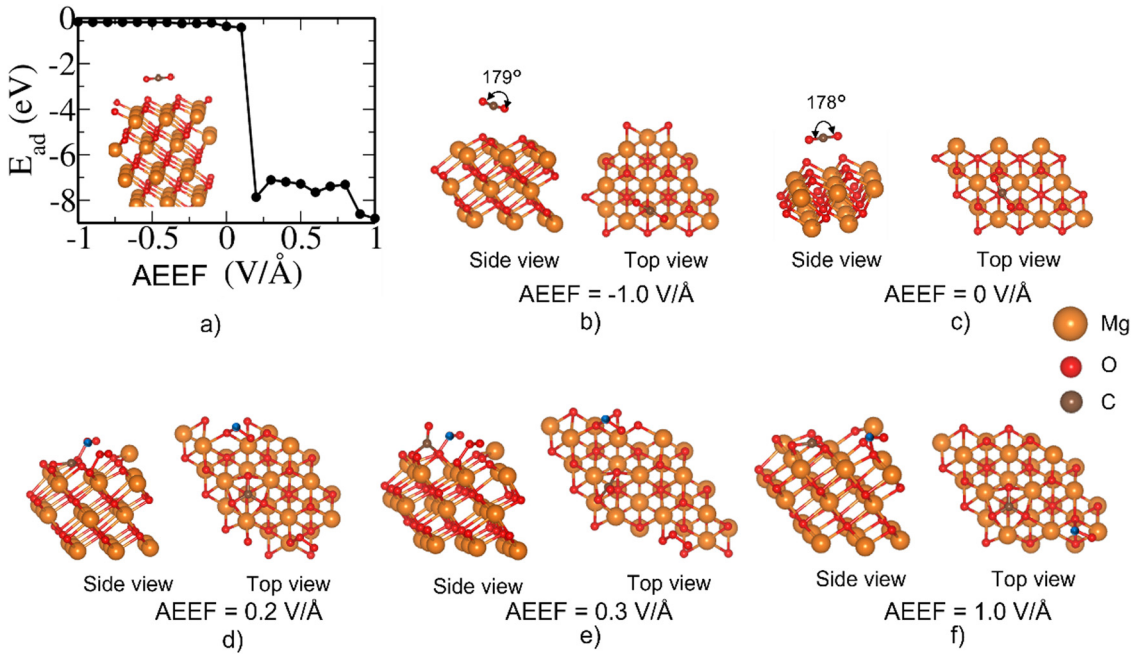

Fig. 11 (a) The variation of E_{ad} (in eV) with AEEF for MgO(111)–O-terminated/CO_2 on the O top site. Relaxed structures of configurations at (b) 0.0 V Å^{-1}, (c) 0.2 V Å^{-1}, (d) 0.3 V Å^{-1}, (e) 1.0 V Å^{-1} and (f) −1.0 V Å^{-1}. The dissociated O from CO_2 in (c) is colored blue.

adsorption energy is also a consequence of the large local reconstruction of the surface (see Fig. 10(c) and (d)). The strong stabilization due to CO_2 dissociative adsorption is an irreversible process in the CO_2 adsorption–desorption behavior.

The dissociation of CO_2 into CO + O is also observed when CO_2 interacts with the top site of the MgO(111)–O surface (Fig. 11). Here too, CO_2 is weakly adsorbed at a low AEEF of $\leq$0.1 V Å^{-1}. Surprisingly, at AEEF = 0.2 V Å^{-1}, there is a large stabilization of E_{ad} of about −8.0 eV. This arises primarily from the local reconstruction of the MgO(111) surface with the surface O atoms protruding out of the surface, as seen in Fig. 11(d). At all the positive AEEF values, the E_{ad} remains below −7.0 eV, corresponding to the highly distorted structure. Such a large stabilization of the E_{ad} is quite unusual for CO_2 adsorption on MgO(111)–O surfaces. The strong dissociative adsorption could imply the irreversible capture of CO_2. Furthermore, this phenomenon indicates that AEEF enhances the activity of the polar MgO(111) surfaces for CO_2 reduction to CO.

Table 1 Summary of the various adsorption and inaccessible sites of CO_2 on MgO surfaces with AEEF ranging from −1.0 to 1.0 V Å^{-1}

Surface and initial site	Final site (H: hollow; B: bridge; Mg: Mg top; and O: O top) and field (AEEF in V Å^{-1})			Inaccessible site
100 B	(a) O site: ($-1 \leq$ AEEF $\leq$ 0.2, bent Mg_2CO_3)	(b) O site: (0.2 $\leq$ AEEF $\leq$ 1.0, comparatively linear CO_2)		H
100 Mg	(a) H site: (AEEF $\leq$ 0, 0.5 $\leq$ AEEF $\leq$ 1.0, linear CO_2)	(b) Mg site: (0.1 $\leq$ AEEF $\leq$ 0.4, AEEF = −0.2, −0.3, −0.9, −1.0, linear CO_2)	(c) O site: ($-0.8 \leq$ AEEF ≤ -0.5, CO_3^{2-} species)	(a) Mg and B, (b) H, (c) H
100 O	(a) H site: (AEEF = 0.2, linear CO_2)	(b) O site: (0.3 $\leq$ AEEF $\leq$ 1.0, linear CO_2)	(c) O site: ($-1.0 \leq$ AEEF $\leq$ 0.1, bent CO_2)	(a) Mg and O, (b) H, (c) H
110 O	(a) O site: ($-1.0 \leq$ AEEF $\leq$ 1.0, bent CO_2)			H
110 Mg	(a) O site: (0.0 $\leq$ AEEF $\leq$ 1.0, $-0.7 \leq$ AEEF ≤ -0.5, bent CO_2)	(b) Mg site: ($-1.0 \leq$ AEEF ≤ -0.8, $-0.4 \leq$ AEEF ≤ -0.1, linear CO_2)		H
110 B	(a) O site: (0.3 $\leq$ AEEF $\leq$ 0.9, CO_3^{2-} species with stronger adsorption)	(b) O site: ($-0.1 \leq$ AEEF$\leq$ 0.2, CO_3^{2-} species with weaker adsorption)		H
111-Mg-terminated Mg	(a) Mg site: ($-0.6 \leq$ AEEF $\leq$ 1.0, linear CO_2)	(b) Mg site: ($-0.9 \leq$ AEEF $\leq$ 0.7, carbonate compound)		H
111-Mg-terminated B	(a) B site: ($-1.0 \leq$ AEEF $\leq$ 0.4, linear CO_2)	(b) Dissociative adsorption (CO + O): 0.5 $\leq$ AEEF $\leq$ 0.8, CO on Mg site		H
111-O-terminated B	(a) B site: ($-1.0 \leq$ AEEF $\leq$ 0.3, linear CO_2)	(b) Dissociative adsorption (CO + O): 0.4 $\leq$ AEEF $\leq$ 1.0		H
111-O-terminated O	(a) Linear CO_2 ($-1.0 \leq$ AEEF $\leq$ 0.1), O site	(b) Dissociative adsorption (CO + O): 0.2 $\leq$ AEEF $\leq$ 1.0		H

4. Summary

The use of AEEF in CO_2 capture on earth-abundant basic oxides such as MgO provides a new opportunity for low-cost and efficient processes for reducing anthropogenic CO_2. In the present work, we have investigated CO_2 adsorption–desorption behavior on various MgO surfaces under AEEFs between −1 to 1 V Å^{-1} using first-principles theoretical analysis. Our results show that (a) the CO_2 'switches' between different metastable states with varying AEEF, and (b) these metastable states are quite distinct depending on the polarity of the MgO surfaces.

In the cases of the non-polar (100) and (110) surfaces of MgO, we mostly observed the formation of carbonate (CO_3^{2-}) species with strong chemisorbed states at negative AEEFs, which switched to weakly adsorbed states at weakly negative or positive values of AEEF. Interestingly, on the polar MgO(111) surface, the CO_2 molecule irreversibly dissociates into CO + O at positive AEEF, indicating the reduction of CO_2 to CO. This manifests the role of AEEF for CO_2 reduction to CO that usually requires high temperature in a thermochemical process. Therefore, different surfaces of MgO can be utilized to capture CO_2, and in some cases, reduce it to CO, through an appropriate choice of AEEF (see Table 1). We have shown that in some cases, the broken inversion symmetry at the adsorption site results in an induced dipole moment, which couples linearly with the AEEF, thereby facilitating electric control of reaction mechanisms and catalytic activity.

Our specific results will stimulate experimental work to explore the influence of applied external electric fields on the adsorption–desorption and reduction of CO_2 on basic oxides to develop low-energy, low-cost sustainable technologies for CO_2 capture and conversion.

Conflicts of interest

There are no conflicts to declare.

Acknowledgements

UVW acknowledges support from Shell India Markets Private Limited and a JC Bose National Fellowship of SERB-DST, and JNCASR. AKN and SS would like to acknowledge Sander van Bavel and Michiel Boele (Shell Global Solutions International B. V.) for the discussions.

References

1 B. Metz, O. Davidson, H. de Coninck, M. Loos and L. Meyer, *IPCC Special Report on Carbon Dioxide Capture and Storage*, Cambridge University Press, UK, 2005, p. 431.
2 T. A. Boden, G. Marland and R. J. Andres, *Global, Regional, and National Fossil-Fuel CO_2 Emissions. Carbon Dioxide Information Analysis Center,* Oak Ridge National Laboratory, U.S. Department of Energy, Oak Ridge, Tenn., USA, 2017.
3 H. Herzog and D. Golomb, *Encyclopedia Energy*, 2004, **1**, 277–287.
4 G. Puxty, R. Rowland, A. Allport, Q. Yang, M. Bown, R. Burns, M. Maeder and M. Attalla, *Environ. Sci. Technol.*, 2009, **43**, 6427–6433.
5 L. Raynal, P.-A. Bouillon, A. Gomez and P. Broutin, *Chem. Eng. J.*, 2011, **171**, 742–752.
6 D. Y. C. Leung, G. Caramanna and M. M. Maroto-Valer, *Renewable Sustainable Energy Rev.*, 2014, **39**, 426–443.
7 S. E. Zanco, J.-F. Pérez-Calvo, A. Gasós, B. Cordiano, V. Becattini and M. Mazzotti, *ACS Eng. Au*, 2021, **1**, 50–72.
8 W. Y. Hong, *Carbon Capture Sci. Technol.*, 2022, **3**, 100044.
9 C. Dhoke, S. Cloete, S. Krishnamurthy, H. Seo, I. Luz, M. Soukri, Y. Park, R. Blom, S. Amini and A. Zaabout, *Chem. Eng. J.*, 2020, **380**, 122201.
10 L. Riboldi and O. Bolland, *Energy Proc.*, 2017, **114**, 2390–2400.
11 F. Raganati, R. Chirone and P. Ammendola, *Ind. Eng. Chem. Res.*, 2020, **59**, 3593–3605.
12 C. A. Grande, R. P. L. Ribeiro, E. L. G. Oliveira and A. E. Rodrigues, *Energy Proc.*, 2009, **1**, 1219–1225.
13 C. A. Grande, R. P. P. L. Ribeiro and A. E. Rodrigues, *Energy Fuels*, 2009, **23**, 2797–2803.
14 Q. Sun, G. Qin, Y. Ma, W. Wang, P. Li, A. Du and Z. Li, *Nanoscale*, 2017, **9**, 19–24.
15 F. Wang, P. Li, S. Wei, J. Guo, M. Dan and Y. Zhou, *Appl. Surf. Sci.*, 2018, **445**, 568–574.
16 H. Xiong, H. Zhang and L. Gan, *J. Mater. Sci.*, 2021, **56**, 4341–4355.
17 B. Liao, Z. Zhang, D. Wang, Y. Xu, Y. Wei, W. Bao, K. Lv, J. Wang and Y. Wang, *Appl. Surf. Sci.*, 2022, **572**, 151312.
18 A. A. Khan, I. Ahmad and R. Ahmad, *Chem. Phys. Lett.*, 2020, **742**, 137155.
19 H. Guo, W. Zhang, N. Lu, Z. Zhuo, X. C. Zeng, X. Wu and J. J. Yang, *J. Phys. Chem. C*, 2015, **119**, 6912–6917.
20 H. Y. Ammar, K. M. Eid and H. M. Badran, *J. Phys. Chem. Solids*, 2021, **153**, 110033.
21 M. Xiao, B. Zhang, H. Song, Y. Lv and B. Xiao, *Solid State Commun.*, 2021, **338**, 114459.
22 D. Biriukov and Z. Futera, *J. Phys. Chem. C*, 2021, **125**, 7856–7867.
23 X. Zhang, H. Li, Z. Xia, S. Yu, S. Wang and G. Sun, *Phys. Chem. Chem. Phys.*, 2021, **23**, 1584–1589.
24 J.-G. Zhou and Q. L. Williams, *J. Phys.: Condens. Matter*, 2009, **21**, 055008.
25 F. Che, J. T. Gray, S. Ha and J. S. McEwen, *ACS Catal.*, 2017, **7**, 551–562.
26 F. Che, J. T. Gray, S. Ha and J. S. McEwen, *ACS Catal.*, 2017, **7**, 6957–6968.
27 F. Che, J. T. Gray, S. Ha and J. S. McEwen, *J. Catal.*, 2015, **332**, 187–200.
28 S. Shaik, D. Danovich, J. Joy, Z. Wang and T. Stuyver, *J. Am. Chem. Soc.*, 2020, **142**, 12551–12562.
29 S. Shaik, R. Ramanan, D. Danovich and D. Mandal, *Chem. Soc. Rev.*, 2018, **47**, 5125–5145.
30 G. Chuah, N. Kruse, W. Schmidt, J. Block and G. Abend, *J. Catal.*, 1989, **119**, 342–353.
31 L. Keller, T. Lohaus, L. Abduly, G. Hadler and M. Wessling, *Chem. Eng. J.*, 2019, **371**, 107–117.

32 K. Sugiura, S. Ogo, K. Iwasaki, T. Yabe and Y. Sekine, *Sci. Rep.*, 2016, **6**, 25154.
33 M. Shetty, M. A. Ardagh, Y. Pang, O. A. Abdelrahman and P. J. Dauenhauer, *ACS Catal.*, 2020, **10**, 12867–12880.
34 Y. Hu, Y. Guo, J. Sun, H. Li and W. Liu, *J. Mater. Chem. A*, 2019, **7**, 20103–20120.
35 M. A. Manae, L. Dheer, S. Rai, S. Shetty and U. V. Waghmare, *Phys. Chem. Chem. Phys.*, 2022, **24**, 1415–1423.
36 S. Arndt, G. Laugel, S. Levchenko, R. Horn, M. Baerns, M. Scheffler, R. Schlögl and R. Schomäcker, *Catal. Rev.*, 2011, **53**, 424–514.
37 J. S. J. Hargreaves, G. J. Hutchings and R. W. Joyner, *Catal. Today*, 1990, **6**, 481–488.
38 H.-X. Fan, T.-Y. Cui, A. Rajendran, Q. Yang, J. Feng, X.-P. Yue and W.-Y. Li, *Catal. Today*, 2020, **356**, 535–543.
39 H. Y. Kim, H. M. Lee and J.-N. Park, *J. Phys. Chem. C*, 2010, **114**, 7128–7131.
40 M. B. Jensen, L. G. M. Pettersson, O. Swang and U. Olsbye, *J. Phys. Chem. B*, 2005, **109**, 16774–16781.
41 S. Jiang, Y. Lu, S. Wang, Y. Zhao and X. Ma, *Appl. Surf. Sci.*, 2017, **416**, 59–68.
42 D. Cornu, H. Guesmi, J.-M. Krafft and H. Lauron-Pernot, *J. Phys. Chem. C*, 2012, **116**, 6645–6654.
43 G. A. Mutch, S. Shulda, A. J. McCue, M. J. Menart, C. V. Ciobanu, C. Ngo, J. A. Anderson, R. M. Richards and D. Vega-Maza, *J. Am. Chem. Soc.*, 2018, **140**, 4736–4742.
44 J. Resasco, L. D. Chen, E. Clark, C. Tsai, C. Hahn, T. F. Jaramillo, K. Chan and A. T. Bell, *J. Am. Chem. Soc.*, 2017, **139**, 11277–11287.
45 W. K. Fan and M. J. Tahir, *Environ. Chem. Eng.*, 2021, **9**, 105460.
46 B. Liang, H. Duan, T. Sun, J. Ma, X. Liu, J. Xu, X. Su, Y. Huang and T. Zhang, *ACS Sustainable Chem. Eng.*, 2019, **7**, 925–932.
47 P. Giannozzi, S. Baroni, N. Bonini, M. Calandra, R. Car, C. Cavazzoni, D. Ceresoli, G. L. Chiarotti, M. Cococcioni, I. Dabo, A. Dal Corso, S. de Gironcoli, S. Fabris, G. Fratesi, R. Gebauer, U. Gerstmann, C. Gougoussis, A. Kokalj, M. Lazzeri, L. Martin-Samos, N. Marzari, F. Mauri, R. Mazzarello, S. Paolini, A. Pasquarello, L. Paulatto, C. Sbraccia, S. Scandolo, G. Sclauzero, A. P. Seitsonen, A. Smogunov, P. Umari and R. M. Wentzcovitch, *J. Phys.: Condens. Matter*, 2009, **21**, 395502.
48 P. E. Blöchl, *Phys. Rev. B: Condens. Matter Mater. Phys.*, 1994, **50**, 17953–17979.
49 J. P. Perdew, A. Ruzsinszky, G. I. Csonka, O. A. Vydrov, G. E. Scuseria, L. A. Constantin, X. Zhou and K. Burke, *Phys. Rev. Lett.*, 2008, **100**, 136406.
50 S. Grimme, *J. Comput. Chem.*, 2006, **27**, 1787–1799.
51 F. Che, J. T. Gray, S. Ha, N. Kruse, S. L. Scott and J. S. McEwen, *ACS Catal.*, 2018, **8**, 5153–5174.
52 H. J. Kreuzer, *Surf. Sci.*, 1991, **246**, 336–347.
53 M. Liu, Y. Pang, B. Zhang, P. De Luna, O. Voznyy, J. Xu, X. Zheng, C. T. Dinh, F. Fan, C. Cao, F. P. G. de Arquer, T. S. Safaei, A. Mepham, A. Klinkova, E. Kumacheva, T. Filleter, D. Sinton, S. O. Kelley and E. H. Sargent, *Nature*, 2016, **537**, 382–386.
54 C. Wolf, **https://christoph-wolf.at/tag/dipfield/**, accessed 21 August 2023.
55 A. Kakekhani and S. Ismail-Beigi, *ACS Catal.*, 2015, **5**, 4537–4545.
56 M. F. Sarott, M. D. Rossell, M. Fiebig and M. Trassin, *Nat. Commun.*, 2022, **13**, 3159.